Journal of Photochemistry & Photobiology, A: Chemistry 441 (2023) 114664

Contents lists available at ScienceDirect

Journal of Photochemistry & Photobiology, A: Chemistry

journal homepage: www.elsevier.com/locate/jphotochem

Photovoltaic characteristics of organic heterocyclic 2,9-dimethyl quinacridone in different solvents using DFT approach

Shradha Lakhera [a], Meenakshi Rana [a,*], Kamal Devlal [a], N. Kanagathara [b], Jan Janczak [c]

[a] Department of Physics, School of Sciences, Uttarakhand Open University, Haldwani 263139, Uttarakhand, India
[b] Department of Physics, Saveetha School of Engineering, Saveetha Institute of Medical and Technical Sciences, Thandalam, Chennai 602105, Tamil Nadu, India
[c] Institute of Low Temperature and Structure Research, Polish Academy of Sciences, Okólna 2 str., 50-442 Wrocław, Poland

ARTICLE INFO

Keywords:
Density functional theory
Nonlinear optics
2,9-dimethyl quinacridone
Photovoltaics, Dye-synthesized solar cells

ABSTRACT

In this work, efforts had been made to develop the photovoltaic utility of 2,9-dimethyl quinacridone (2,9-DMQA) using density functional theory (DFT). Initially, the structural analysis was done using the molecule's ground state geometry to study the molecule's structural characteristics. In particular, the global reactivity descriptors, density of states (DOS) analysis, molecular electrostatic potential (MEP), contour plot, and, ionization potential surface, dipole moment, Mulliken, and natural charge distribution, were computed and analyzed to identify the nucleophilic and electrophilic sites of the molecule. Considering N – H the donor and C = O the acceptor group, the intramolecular charge transfer (ICT) was established. Hirshfeld surfaces and fingerprint plots were also determined to explore intermolecular interactions. The electronic transitions were analyzed using the simulated absorption and emission spectra. To better understand the role of solvents in inducing the photovoltaic property, the light-harvesting efficiency of the molecules was computed in the considered solvents. The title molecule provided light harvesting efficiency in order of chloroform > ethanol > cyclohexane. Other photovoltaic properties were also computed to predict the power conversion efficiency of the molecule. Consequently, the title molecule offers a strong charge conduction ability and effective electron transport from the donor to the acceptor. The obtained results were favorable enough to test experimentally 2,9-DMQA which could be used as a photosensitizer in dye-synthesized solar cells and could enhance the performance of organic photovoltaic cells.

1. Introduction

Solar energy is the most abundant and renewable source of energy currently date. Along, it is an advantageous alternative to fossil fuels and non-renewable resources [1]. Over the past decades, the scientific industry had been heading towards the development of materials of utility that can make a maximum of solar energy into use. That's why exploring materials with enhanced photovoltaic properties had been a considerable and specific field of research for many researchers and scientists. Materials with such utility are the leading elements in several applications including solar cells, photodiodes, laser diodes, LEDs, optical communication systems, optical storage, and remote sensing systems [2]. Along with the high absorbance rate, the photovoltaic materials must be environment-friendly, low-cost, easily available, easily fabricated, flexible to the researcher, and many more [3]. Using solar energy as a substitute for fossil fuels will help decrease greenhouse gas production and global warming [4]. Generally, approximately 173,000 terawatts of solar energy are continuously received by the earth's surface [5]. To use this energy up to its optimum, solar panels aided with high solar conversion efficient technology can be installed at every possible place [6]. Silicon solar cells have been considered the most used inorganic photovoltaic technology. But they have certain disadvantages with their price and complicated fabrication procedures [7]. Dye-synthesized solar cells (DSSCs) overcome such disadvantages. For instance, DSSCs had been the most followed mode due to their durability, flexibility, relatively low cost, high-power conversion efficiency,

Abbreviations: DFT, Density Functional Theory; DSSC, Dye Synthesized Solar Cell; NLO, Non-Linear Optics; 2,9-DMQA, 2,9-Dimethyl quinacridone; PCE, Power Conversion Efficiency; CCDC, Cambridge Crystallographic Data Centre; IEFPCM, Integral Equation Formalism-Polarizable Continuum Model; SCRF, Self-Consistent Reaction Field; HOMO, Highest Occupied Molecular Orbital; LUMO, Lowest Unoccupied Molecular Orbital; NBO, Natural Bond Orbital; DOS, Density Of States; TDM, Transition Density Matrix; LHE, Light Harvesting efficiency; FF, Fill factor; ICT, Intramolecular Charge transfer; MEP, Molecular Electrostatic Potential.

* Corresponding author.
E-mail address: mrana@uou.ac.in (M. Rana).

https://doi.org/10.1016/j.jphotochem.2023.114664
Received 9 January 2023; Received in revised form 23 February 2023; Accepted 5 March 2023
Available online 8 March 2023

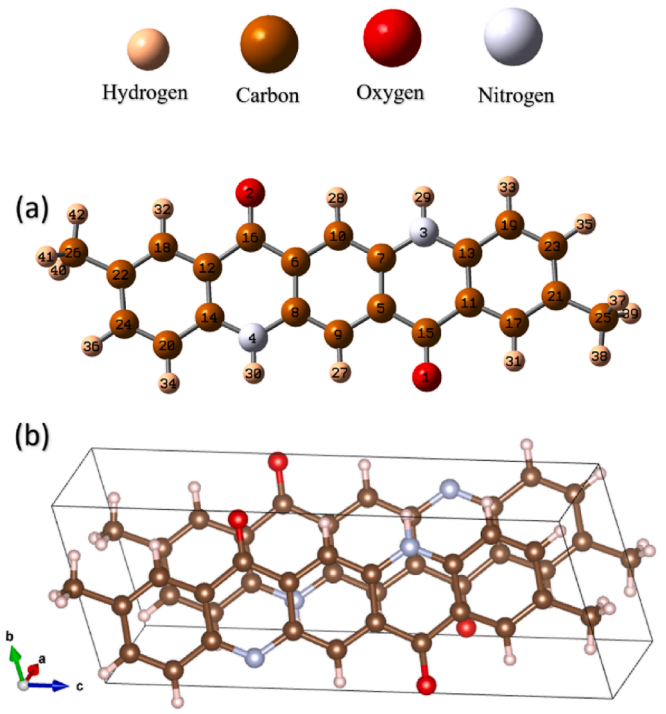

Fig. 1. (a) Optimized geometry of 2,9-DMQA with B3LYP/6–311++G(d,p) basis set, (b) Crystal structure of 2,9-DMQA showing the arrangements of the molecules within the unit cell and the orientation of the unit cell in accordance with the Cartesian coordinates.

eco-friendly, and easy production procedure benefits [8]. Additionally, organic solar cells can be synthesized by simple and inexpensive techniques such as spin coating, spray deposition, printing, etc [9]. Different kinds of organic materials like polymers, organic dyes, plant extracts, etc. are employed to construct efficient and comparatively reliable solar cells [10]. But despite some major benefits over the inorganics, organic solar cells do face some complications. The literature so far reports that the class of organic molecules has considerably improved the power conversion efficiency (PCE), which can reach values close to 8% for a single-junction solar cell but the advancement of the hereto-junction in the solar cell was reported to give PCE up to 10.1% [11]. Thus, to gain the maximum open-circuit voltage (V_{OC}) out of the solar cell, hereto-junction solar cells were established employing different hole transport and electron transport layers to prevent hole-electron recombination decay [12]. The introduction of donor–acceptor bridged systems combined with organic, inorganic, or hybrid compounds has been a revolutionary area in the field of optoelectronics. Linear acceptor–donor–acceptor and acceptor-π-donor-π-acceptor groups like 1,1-dicyanomethylene-3-indanone end-capped non-fullerene systems have been considered areas in the progression of the organic solar cells [13]. Studies were done to report the potent electron-withdrawing thiazole rings used as a bridged unit in the design of the small molecular electron acceptor. Such designs with indacenodithiophene as core and 1,1-dicyanomethylene-3-indanone as an end-capped unit, and thiazole ring as spacers were observed to exhibit the power conversion efficiency of more than 5% [14]. Fullerene-free acceptor molecules are efficiently utilized in organic solar cells due to their perfect symmetry with donor polymers. One such study was done by M. Haroon and their team using DFT tools [15]. One new approach of end-capped designing proved efficient in developing highly efficient organic solar cells with high open circuit voltage. Non-fused ring electron acceptors with different end-capped substituents were designed to construct efficient organic solar cells [16]. Along with the experimental research, various computational physicists have tried to identify some "*magic compounds*" that can enhance the PCE up to the maximum. Such computational estimations have been studied for organic molecules using Density functional theory (DFT). A close inspection reveals that the DFT and time-dependent density-functional theory (TD-DFT) computations have been extensively used for the pre-evaluation of photovoltaic properties of compounds. Computational studies have been significantly important and laid the basis for many experimental studies. Computational studies may give further insight into principles for charge-generation processes and carrier-transport properties of organic molecules which can be considered potential candidates for photovoltaic devices. The literature has accounted for the application of the DFT basically for the conjugated systems. This might be due to the connected p-orbitals with delocalized electron density which is responsible for the increased stability and reactivity of the molecules. The availability of alternate single and double bonds leads to high absorption cross-section and induces the photon-excitation on exposure to visible light. A similar kind of conjugation was observed in a previously done study for the enhancement of Nonlinear optical (NLO) activity of the 2-dinitrotoluene (2NT) after the substitution of the halogens (F, Cl, Br, and I) at the para position of the benzene ring [17]. The conjugation in the toluene ring was found responsible for the increased value of the first-order hyperpolarizability of the compound. Essential amino acids were also employed for the non-linear optical properties using the DFT approach [18]. This also might be due to the high dipole moments and bond conjugation of the essential amino acids. The linearly connected benzene rings of the Luteolin lead to the high chemical reactivity of the organic derivative from *Tridax Procumbens*. Conjugation is considered the basis of chemical reactivity as the conjugated structure of luteolin was further employed as a potent anti-cancerous agent against breast cancer by *in-silico* approach [19]. Studies have been cited in the literature reporting the power conversion efficiency of the solar cell is more than 22% with the help of the materials having an efficient narrow gap between the donor and acceptor moieties [20]. Moreover, fullerenes, non-fullerenes, and inorganic nanoclusters complexes have also gained considerable attention in the field of optoelectronics [21–23]. Aromatic organic compounds are generally used as a pigment for industrial colorant applications such as robust outdoor paints, inkjet printer ink, tattoo ink, water colors, laser printer toner, etc [24]. QA and its derivatives are colored due to the availability of N-H…O intermolecular hydrogen [25]. Additionally, the hydrogen bond of the QAs has polymer-like stability. A relatively higher power conversion efficiency of quinacridone. A study done by H. Meier and W. Albrecht reported that 2,9-DMQA has a radiative lifetime equal to 10^{10} cm^{-1} V^{-1} and diffusion lengths up to 100 Å [26]. The higher value of diffusion length indicates that an excited carrier will travel up to 100 Å before recombining [26]. A hetero-junction solar cell with CdS deposited on a glass substrate by electrochemical deposition method designed by K. Manabe and team reported V_{OC} of 0.61 V and short-circuit photocurrent of 127μA/cm^2 with a large fill-factor [27]. Followed by the extraordinary V_{OC}, no exhaustion was observed over a month with continuous irradiation of 15 mW/cm^2 [27]. Thus, the reference studies were the motivation behind the selection of the title compound as the photosensitizing material.

In this novel research study, the photovoltaic characteristics of 2,9-DMQA were investigated using DFT and TD-DFT approaches. The molecular characteristics, intramolecular interactions, molecular electrostatic potential, and charge transport characteristics were studied to enhance the performance of the hetero-junction organic solar cell. The electronic properties of the title molecule were studied in different solvents. Charge transfer and intramolecular interactions were studied by Hirshfeld analysis and density of state analysis. The behavior of 2,9-DMQA as a photosensitizing dye with TiO_2 as an ideal semiconductor for charge transport was studied by analyzing the nature of adsorption between 2,9-DMQA and TiO_2.

2. Computational methods

The 3-D structure of 2,9-DMQA was downloaded from the online

Table 1
Computed global reactivity parameters for 2,9-DMQA in different considered solvents.

Molecular property	Gas	Chloroform	Cyclohexane	Ethanol
Ionization potential (*IP*)	5.52	5.56	5.53	5.59
Electron affinity (*EA*)	2.51	2.65	2.58	2.66
Chemical potential (μ)	−4.01	−4.10	−4.05	−4.12
Electronegativity (χ)	4.01	4.10	4.05	4.12
Hardness (η)	1.5	1.45	1.47	1.46
Softness (S)	0.66	0.68	0.68	0.68
Electrophilicity index (ω)	5.36	5.79	5.57	5.81
Electron accepting power (ω^{+})	3.53	3.92	3.73	3.92
Electron donating power (ω^{-})	7.55	8.02	7.78	8.05

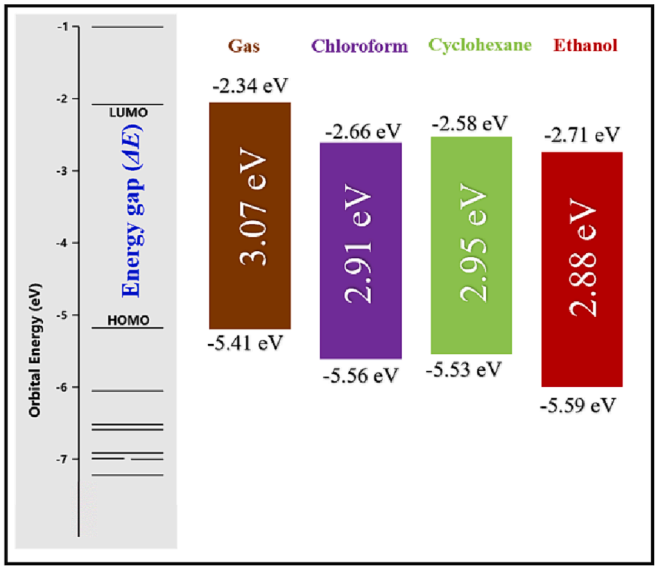

Fig. 2. HOMO-LUMO energies and the ΔE for 2,9-DMQA in different considered solvents.

database PubChem (https://pubchem.ncbi.nlm.nih.gov/compound/70423) (PubChem ID: 70423). The crystal structure of 2,9-DMQA was downloaded from Cambridge Crystallographic Data Centre (CCDC) (https://www.ccdc.cam.ac.uk/) with CCDC number: 203,604 and crystallographic parameters a = 3.865 Å, b = 6.375 Å, c = 15.78 Å, α = 93.94°, β = 91.51°, and γ = 100.00° (Fig. 1 (b)). The file conversions for different purposes were done using Open Babel software (https://openbabel.org/wiki/Main_Page) [28]. The method of DFT was used for the electronic calculations and the chemical reactivity of the title molecule. All the quantum chemical calculations and spectral analysis were performed employing the DFT in Gaussian 09 program's package (https://gaussian.com/) [29] and the analysis of the chemical and spectral properties was analyzed using Gauss View (https://gaussian.com/gaussview6/) and Gauss Sum (https://gausssum.sourceforge.net/). The geometry of 2,9-DMQA was optimized using B3LYP/6–311-G(++d,p) set of functions in the gas (ε = 1.00) phase and geometry optimization for solvents like Chloroform (ε = 4.72), Cyclohexane (ε = 2.01), and Ethanol (ε = 24.85) was carried out using B3PW91/Lanl2dz [30]. The former basis set is the most precise set of functions for organic compounds. The latter considered set of basis functions is a widely preferred and most accurate set of functions for the ground state and excited state calculations of the organic molecules or systems exposed to solvents. The convergence parameters were set on maximum force as 0.00045, RMS force as 0.0003, maximum displacement as 0.0018, and RMS displacement as 0.0012 for structure minimization. The same set of functions was also used for calculating the electronic spectra of 2,9-DMQA in selected solvents using the integral equation formalism-polarizable continuum model (IEFPCM) model to create the solute cavity with the self-consistent reaction field (SCRF) solvent method. The RMS density matrix at 1.00×10^{-8} and the maximum density matrix at 1.00×10^{-6} were used for TD-SCF calculations without any additional set of information. For calculating the emission spectra, optimization of the excited state of interest using TD-DFT was done with keyword #opt td=(nstates = 9,root = 1)b3pw91/lanl2dzscrf=(iefpcm,solvent = chloroform/cyclohexane/ethanol,read) geom = connectivity. The molecular potential and orbital maps were drawn using Spartan software (https://store.wavefun.com/Spartan_Software_s/12.htm) [31]. These maps were used to identify the nucleophilic and electrophilic sites of the 2,9-DMQA. The global reactivity descriptors were employed to develop the intramolecular interactions in the title molecule using energies of the highest occupied and lowest unoccupied molecular orbital (HOMO-LUMO). HOMO is responsible for possessing the valance electrons and LUMO is responsible for possessing the electrons that are excited during electronic transitions. Reactivity parameters were computed using Koopman's equations described in DFT [32]:

$$\Delta E = E_{LUMO} - E_{HOMO} \tag{1}$$

$$IP = -E_{HOMO} \tag{2}$$

$$EA = -E_{LUMO} \tag{3}$$

$$\mu = \frac{E_{HOMO} + E_{LUMO}}{2} \tag{4}$$

$$\chi = \frac{(IP + EA)}{2} \tag{5}$$

$$\eta = \frac{E_{LUMO} - E_{HOMO}}{2} \tag{6}$$

$$S = \frac{1}{\eta} \tag{7}$$

$$\omega = \frac{\mu^2}{2\eta} \tag{8}$$

$$\omega^{+} = \frac{(IP + 3EA)^2}{16(IP - EA)} \tag{9}$$

$$\omega^{-} = \frac{(3IP + EA)^2}{16(IP - EA)} \tag{10}$$

The donor–acceptor interactions were explained using the second-order perturbation Fock– matrix and Mulliken charge distribution. Stabilization energy ($E(2)$) corresponding to each donor (i) and acceptor (j) atom was computed using the below-given equation:

$$E(2) = \Delta E_{ij} - q_i \left(\frac{f_{ij}^2}{E_j - E_i} \right) \tag{11}$$

where $F(i,j)$ -Fock matrix element between i and j NBO orbitals, E_j and E_i are the energies of the acceptor and donor NBOs. The Density of states (DOS) analysis was done to account for the average space of the various states occupied by the system. The DOS spectra were also obtained employing the Gauss Sum software [33]. The nature of electron-withdrawing and donating regions was studied and reported by a transition density matrix (TDM) map and it was drawn using Multiwfn software [34]. TDM was particularly useful in understanding the nature of electron excitation within the molecule. The checkpoint file generated by the ground state optimization of the title molecule from Gaussian was converted into a formatted checkpoint file and was used as the input file for multiwfn in order to generate a TDM plot and isosurface.

As a photosensitizing material works as an ideal absorber of light and

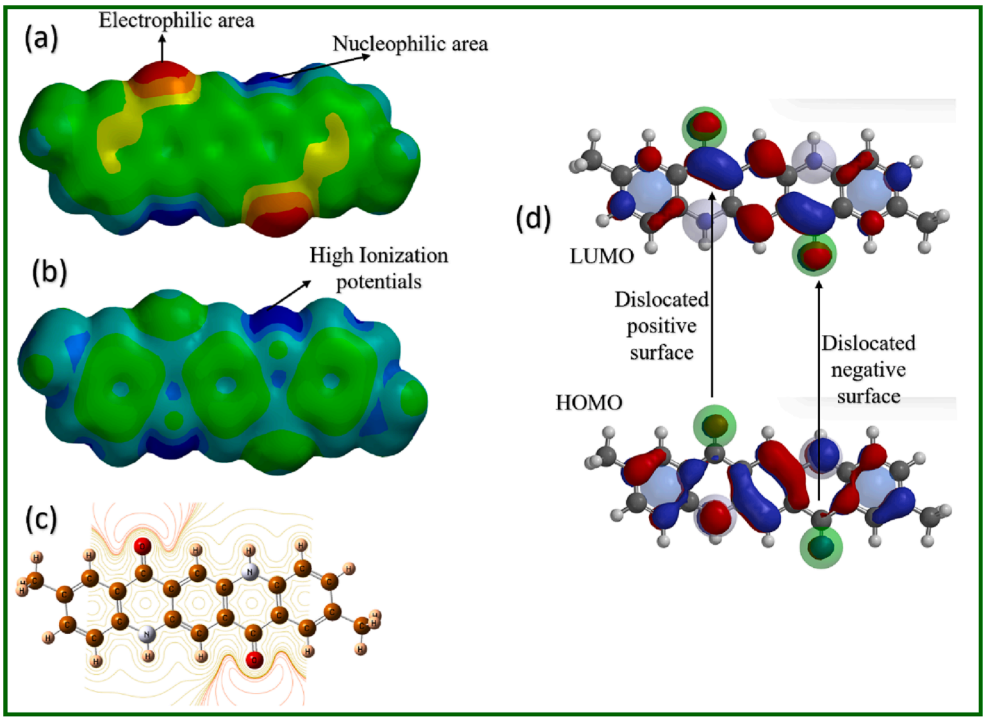

Fig. 3. (a) MEP surface, (b) Ionization potential surface, (c) Contour plots of 2,9-DMQA molecule, (d) HOMO-LUMO map of 2,9-DMQA showing the dislocation of the negative and positive surfaces towards the electrophilic and nucleophilic surface respectively.

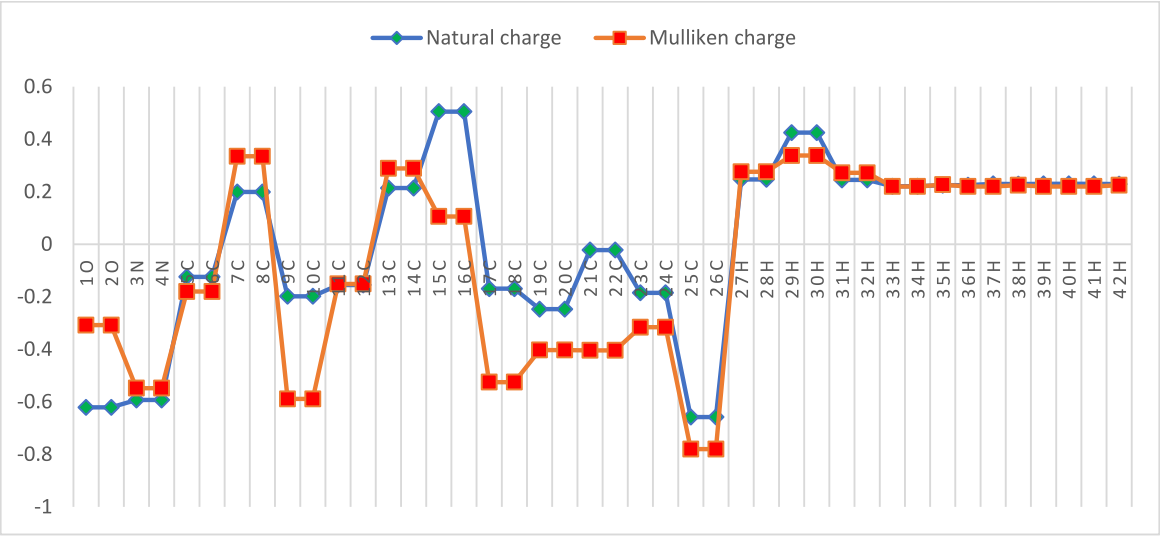

Fig. 4. Mulliken charge and natural charge distribution of 2,9-DMQA.

transfers the absorbed light to a semiconductor in DSSC, it must be of high absorbing efficiency. Thus, the potentiality of the material to absorb light and transfer to a semiconductor is defined as the Light Harvesting Efficiency (LHE) of that material. The LHE is the function of the Oscillator strength (f) of the crucial transition (transition having the highest oscillator strength) of the absorption spectra, it was computed for all the solvents as [35]:

$$E = 1 - 10^{-f} \tag{12}$$

The estimation of the radiative or non-radiative nature of the transitions, radiative lifetime (τ) was calculated using formula [36]:

$$\tau = \frac{c^3}{2fE^2} \tag{13}$$

where c is the speed of light, f and E are the oscillator strength and the excitation energy of the crucial transition (transition having larger value of f obtained in the emission spectra). The value of τ reveals whether the molecules emit radiation during the transitions or the transitions are non-radiative [37].

The interactions between the title compound and Titanium dioxide (TiO_2) have been calculated using equation (14) to figure out the feasibility of electronic injection from dyes to the TiO_2 surface [38].

$$E_{int} = E_{complex} - \left(E_{Tio_2} + E_{2,9-DMQA}\right) \tag{14}$$

Table 2
Second Order Perturbation Theory Analysis of Fock Matrix in NBO Basis of 2,9-DMQA (LP- lone pair, LP*- anti-bond lone pair, BD-bonding orbital, BD*-antibonding orbital, CR-one center core pair, RY- Rydberg orbital).

S. no.	Donor NBO *(i)*	Acceptor NBO *(j)*	*E(2)* (kcal/mol)	*E(j)-E (i)* (au)	*F(i,j)* (au)
1	BD (1) C 18 - H 32	RY*(8) C 24	14982.47	0.02	0.523
2	BD (1) C 22 - C 26	RY*(17) C 26	5668.66	0.15	0.823
3	BD (1) C 26 - H 42	RY*(9) C 6	3386.50	0.03	0.300
4	CR (1) C 18	RY*(14) C 18	18710.66	0.23	1.836
5	CR (1) C 19	RY*(2) H 32	24209.36	0.11	1.456
6	CR (1) C 22	RY*(14) C 18	23752.15	0.17	1.809
7	CR (1) C 22	RY*(13) C 25	6314.71	0.58	1.711
8	CR (1) C 26	RY*(14) C 12	6447.42	2.73	3.745
9	CR (1) C 26	RY*(7) C 14	7072.77	2.33	3.626
10	CR (1) C 26	RY*(11) C 18	2577.30	5.83	3.460
11	CR (1) C 26	RY*(14) C 18	65660.38	0.26	3.672
12	CR (1) C 26	RY*(13) C25	6259.50	2.08	3.219
13	CR (1) C 26	RY*(13) C25	21665.48	0.67	3.392
14	CR (1) C 26	RY*(13) C26	4290.69	3.88	3.641
15	CR (1) C 26	RY*(1) H 33	2155.48	4.20	2.686
16	CR (1) C 26	BD*(1) C 23 - H 35	2027.9	8.72	3.766
17	CR (1) C 26	BD*(1) C 26 – H 41	2938.25	7.81	4.285
18	LP (1) N 4	RY*(11) O 2	4896.23	0.02	0.276
19	LP (1) N 4	RY*(4) C 10	1918.06	0.02	0.196
20	BD*(2) C 18 - C 22	RY*(14) C 14	2538.02	0.04	0.764
21	BD*(2) C20 - C 24	RY*(17) C 26	1856.89	0.21	1.449

where E_{int} is the interaction energy between the 2,9-DMQA and TiO_2, $E_{complex}$ is the ground state energy of the optimized geometry of 2,9-DMQA + TiO_2, E_{TiO2}, is the ground state energy of the optimized geometry of TiO_2, and $E_{2,9\text{-}DMQA}$ is the ground state energy of the optimized geometry of 2,9-DMQA.

The adsorption energy between 2,9-DMQA and TiO_2 was also computed using the following expression [39]:

$$E_{adsorption} = \frac{\left(n \times E_{dye} + E_{TiO2} - E_{dye}\right)}{n} \tag{15}$$

where E_{dye} is the ground state energy of the optimized geometry of 2,9-DMQA, and n is the number of dyes i.e., 1 in our case.

The PCE was also estimated for the title molecule to investigate the efficiency of various photovoltaic cells for a particular molecule and it can be written as equation (16) in terms of short-circuit current density (J_{SC}), open circuit voltage (V_{OC}), incident light power (P_{in}) and fill factor (*FF*) [40]:

$$PCE = \frac{J_{sc} V_{oc} FF}{P_{in}} \tag{16}$$

V_{oc} can be evaluated using the energy difference between the HOMO and LUMO energy as [41,42]:

$$V_{oc} = \left(\left|E_{LUMO}(Donor) - E_{CB}(Acceptor)\right|\right) \tag{17}$$

E_{LUMO} is the energy of the highest occupied molecular orbital of donor moiety (say dye) and E_{CB} is the energy of the lowest unoccupied molecular orbital of acceptor moiety (say TiO_2).

The fill factor (*FF*) is the major parameter that is usually computed to measure the quality of the solar cell. Physically, it is the ratio of the actual maximum obtainable power to the product of short circuit current and open circuit voltage. Computationally, Equation (18) was used to compute the *FF* for the title molecule in different solvents [43]:

$$FF = \frac{V_d - ln(V_d + 0.72)}{V_d + 1} \tag{18}$$

where V_d is a dimensionless voltage computed by below-given equation (19):

$$V_{d=\frac{eV_{OC}}{nK_BT}} \tag{19}$$

where e is the elementary charge with value 3×10^{-8} e, V_{OC} is the open circuit voltage, K_B is the Boltzmann constant and T is the temperature 298.5 K. n is the ideal factor for a diode having ideal value n = 1.

3. Results and discussion

3.1. Optimized geometry and global reactivity descriptors analysis

2,9-DMQA is an aromatic compound having five-linearly bonded benzene rings with methyl groups bonded at the corner benzene rings (Fig. 1 (a)). One C = O and one N – H group is attached to the second and fourth benzene ring (from left to right) in trans directions. The optimized structure of 2,9-DMQA was linear through the benzene chain. 40H – 26C – 41H and 37H – 25C – 39H are the only non-planar angles in the geometry. On optimization, lower bond lengths were obtained for C – H bonds. The higher bond length was observed for the C – C bonds (SD 1). The highest bond lengths were observed for the C – C bonds attached to the methyl groups at the corner most benzene rings (21C – 25C and 22C – 26C). The bond lengths of 1O = 15C and 2O = 16C were observed as 1.26 Å. 3 N – 29H and 4 N – 30H are found to be 1.01 Å. The bond angles between 1O = 15C – 11C, and 2O = 16C – 12C were of the highest magnitude (122.62). The variation in the bond order of C = O and N – H bonds shows the intramolecular interactions within the 2,9-DMQA and the contribution of C = O and N – H in intramolecular interactions. Global reactivity descriptors were computed for the title molecule in a gas, chloroform, cyclohexane, and ethanol. The energies corresponding to the molecular orbitals (HOMO-LUMO) were computed to establish the molecule's chemical reactivity in different selected phases (Table 1). The band gap (ΔE) between the HOMO-LUMO in different solvents has been illustrated in Fig. 2. Among all the solvents, the value of ΔE was lowest for ethanol. The lower *EA* and higher *IP* are determining the eventual charge transfer within the molecule which influences their high polarizability. The high value of χ for ethanol describes the tendency of functional groups to attract electrons toward themselves. The electrophilicity index (ω) is the indication of an atom or molecule containing an electron pair available for bonding. The value of ω was highest for the title molecule in ethanol. This enhances the reactivity of the title molecule in ethanol solvent. The ω^+ and ω^- values for 2,9-DMQA in solvents indicate the induced ICT in the title molecule in solvent phases as compared to the gas phase. Therefore, it can be said that the solvents better impart in inducing ICT in the title molecule.

3.2. Molecular electrostatic potential and charge analysis

MEP surface is used to illustrate the intramolecular interactions of molecules. MEP surface consists of the colored 3-D surface having a color sequence from red < yellow < green < light blue < dark blue [44,45]. This indicates the most electronegative region towards the most electropositive region i.e., red colored surface is the most electronegative, and blue colored region is the most electropositive moiety [46]. MEP surfaces allow visualizing the charge distributions of molecules, being very useful for evaluating electrostatic interactions between molecules, such as hydrogen bonds (H-bonds). The MEP surface of 2,9-DMQA illustrated in Fig. 3(a) indicates that the red-colored surface is spread over the C = O groups and the blue-colored regions over the N – H bonds. As the N – H bonds are electron-donating due to the nucleophilic nature of nitrogen atoms and C = O are electron-accepting due to the

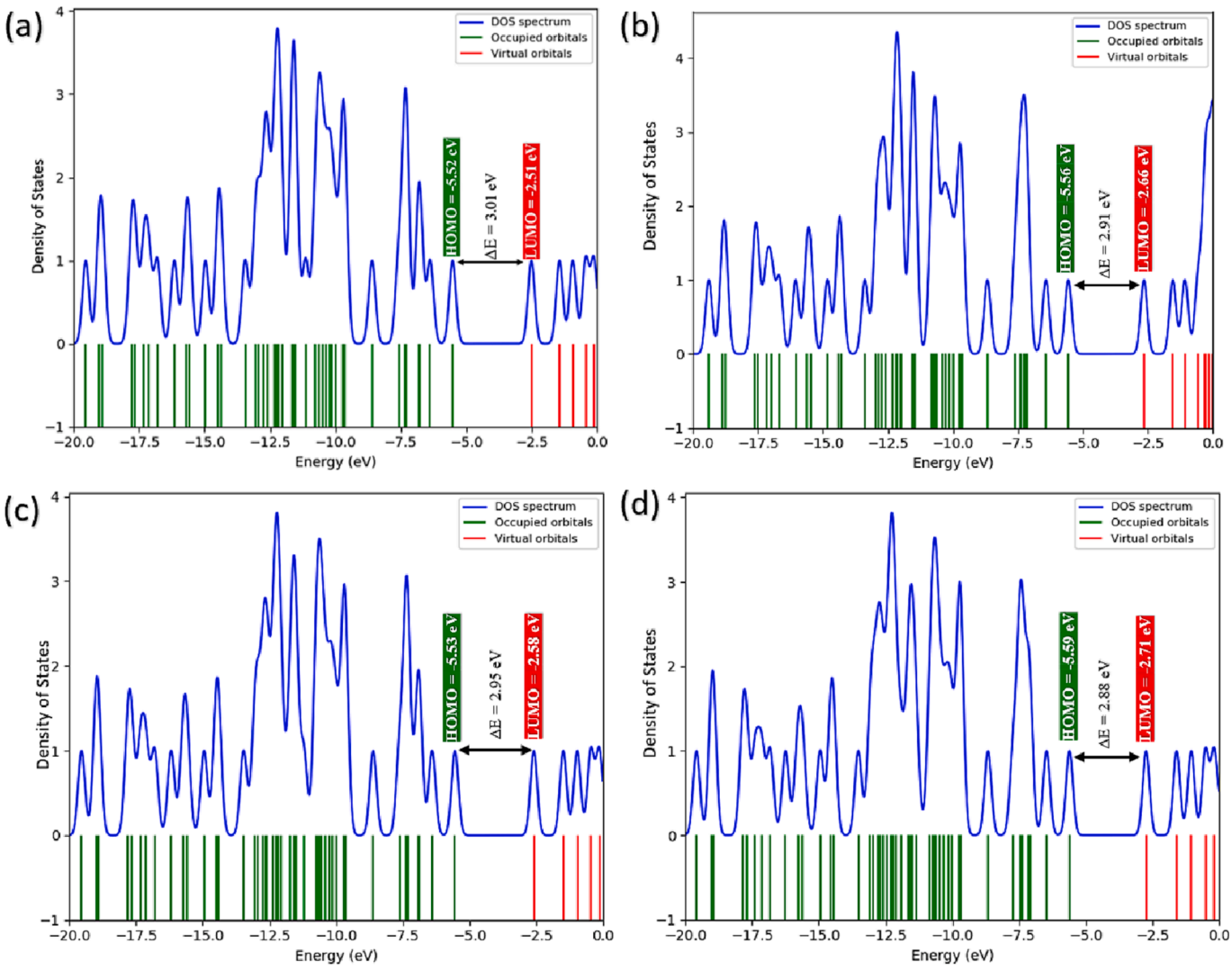

Fig. 5. The density of states (DOS) of 2,9-DMQA in (a) gas, (b) chloroform, (c) cyclohexane, and (d) ethanol.

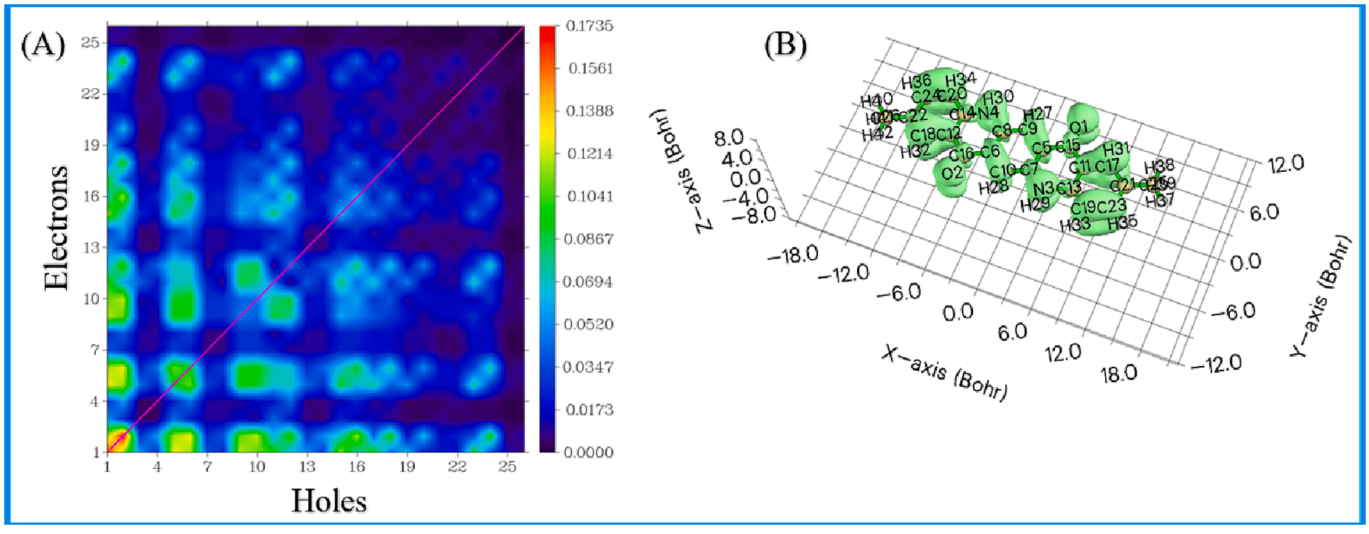

Fig. 6. **(A)** Transition density matrix plot of 2,9-DMQA, **(B)** Isosurface of the 2,9-DMQA.

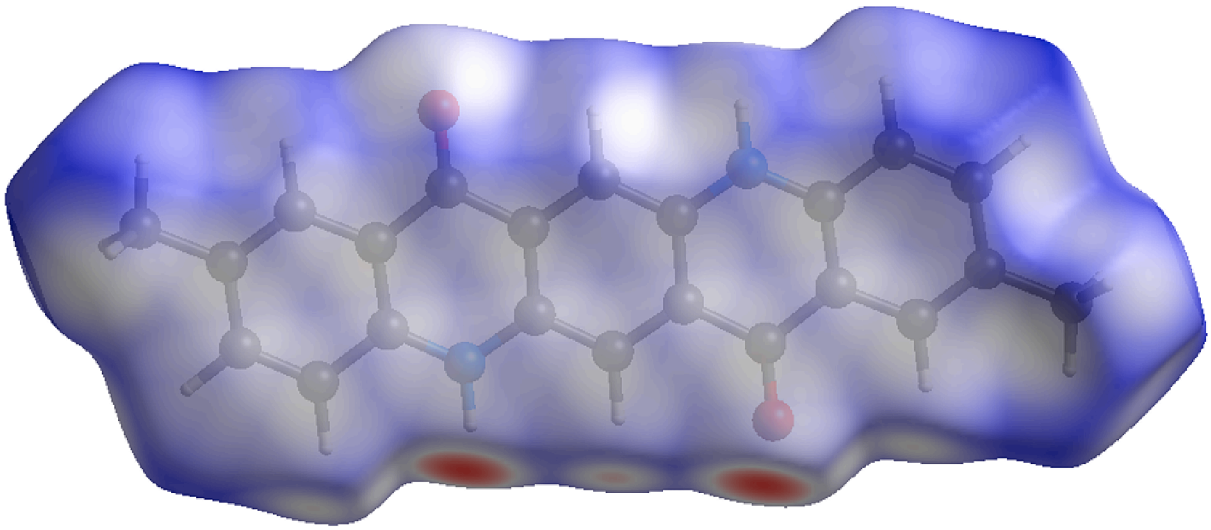

Fig. 7. Hirshfeld surface of 2,9-DMQA. Red color indicates the greatest contributing interactions and blue color indicates the small contributory parts in the intermolecular interactions. (For interpretation of the references to color in this figure legend, the reader is referred to the web version of this article.)

electrophilic nature of the oxygen atom. Thus, the MEP surface identifies the donating nature of N – H bonds and the accepting nature of C = O bonds of the 2,9-DMQA. These regions are the reactive sites of the molecule and are active for intramolecular interactions. The *IP* map (Fig. 3(b)) was computed to predict the location of the *IP*-rich and deficient moieties. The blue color in the *IP* map indicates the moieties with high *IP* which is spread over the N – H bonds of the geometry. Moiety with high *IP* has a high charge-transferring tendency [30]. Thus, the *IP* surface shows that N – H bonds of 2,9-DMQA are highly active in transferring the charge cloud. The green color of the *IP* surface indicates the region with intermediate *IP*. As 2,9-DMQA is the molecule with a high value of *IP*, there is no trace of the red regions (the region with a low value of *IP*) in the *IP* surface of 2,9-DMQA. The contour plots were also determined for the title molecule to identify the regions under the greater influence of the electric field [47]. The contour plots comprise the accumulation of contour lines nearby the moieties of the molecule that experience the electric field at the maximum (Fig. 3(c)). The contour lines of the 2,9-DMQA were heavily accumulated nearby the C = O bonds, which shows the chemical reactivity of the molecule. The *IP* surface and the contour plot of the title molecule were in great agreement with the MEP surface and signify N – H and C = O bonds as chemically reactive for inducing the intramolecular interactions. Fig. 3 (d) illustrates the distribution of HOMO-LUMO surfaces over the geometry of 2,9-DMQA. The red color indicates the negative charge and the blue color indicates the positive charges of the functional groups of 2,9-DMQA. In HOMO, the surfaces over the N – H groups have been dislocated and in LUMO, the blue color surfaces were settled over the N – H groups. This shows the nucleophilic nature of the N – H groups. Similarly, any negative surface is absent over the C = O bonds in HOMO, but in LUMO the presence of red surfaces over the C = O bonds was observed. Thus, the HOO-LUMO surfaces distribution illustrates the transfer of charge cloud from the N – H bonds towards the C = O groups. Moreover, the observations of HOMO-LUMO surfaces were in accordance with the MEP surface. Fig. 4 illustrates the comparison of the charge distribution of the atoms of 2,9-DMQA. The charge distribution shows the positive charge contribution of hydrogen atoms and the negative charge contribution of oxygen and nitrogen atoms. The carbon atoms impart positively as well as negatively to the total charge of the molecule. It was observed that the 7C, 8C, 13C, and 14C atoms were bonded to the nitrogen atoms and shows a positive charge. The 15C, and 16C atoms attached to the 1O and 2O respectively also hold positive charges. Apart from these, all the remaining carbon atoms attached to the hydrogen atoms impart negatively to the total charge of 2,9-DMQA. A huge variation of the charge was observed in the N – H and C = O bonds which indicates the involvement of the aforementioned groups in inducing the ICT. The natural bond orbital calculations were done using the second-order perturbation theory of the Fock Matrix. Stabilization energy was computed for all the intramolecular interactions and the interactions with higher values were listed in Table 2. The major interactions were found to be between C…C interaction between one centre core paired electrons and Rydberg electrons. The lone pair of electrons from 4N was shifted to the Rydberg orbital of 2O with a stabilization energy of 4896.23 kcal/mol. The NBO analysis indicates the active participation of 26C, 18C, 4 N, and 2O atoms in ICT. This is also in good agreement with the MEP surface as the reactive sites were along the N and O atoms.

3.3. Density of states analysis

The DOS diagram was plotted using the Gauss sum program to predict the location of the electron density in the 2,9-DMQA in the gas phase, and other considered solvents and the plots have been shown in Fig. 5. DOS plot of 2,9-DMQA in the gas phase shows the occupied orbitals closest to the energy gap consisting of two groups of energy levels. The π orbitals group around −5.52 eV are highly accumulated due to N – H bonds whereas in the π* orbitals around −2.5 eV such contributions due to C=O bonds are negligible. For the lowest unoccupied orbitals, the density contribution is very small. Similar to DOS in the gas phase, the DOS plot of the title molecule in all the solvents shows the high density of electrons along the HOMO and the low density of electrons around LUMO. This reflects the probability of the charge cloud dissociating from the HOMO to LUMO. Moreover, the DOS plots of 2,9-DMQA in gas and solvent phases indicate the existence of typical $\pi \rightarrow \pi^*$ transitions. The location of HOMO-LUMO in the DOS map is in agreement with the HOMO-LUMO values obtained by Koopman's theorem in reactivity descriptors analysis. Thus, DOS analysis indicates the availability of an electron cloud in the title molecule for inducing the electron transfer process.

3.4. Transition density matrix and isosurface analysis

Transition density matrix plots are used for locating the hole and electron density in the molecule [48]. It is used for the interpretation of the electronic excitation processes in molecules. Excitation of the electrons is defined as hole → electron transition [23]. The index range of hydrogen atoms in 2,9-DMQA is 27 to 42. The hydrogen atoms do not

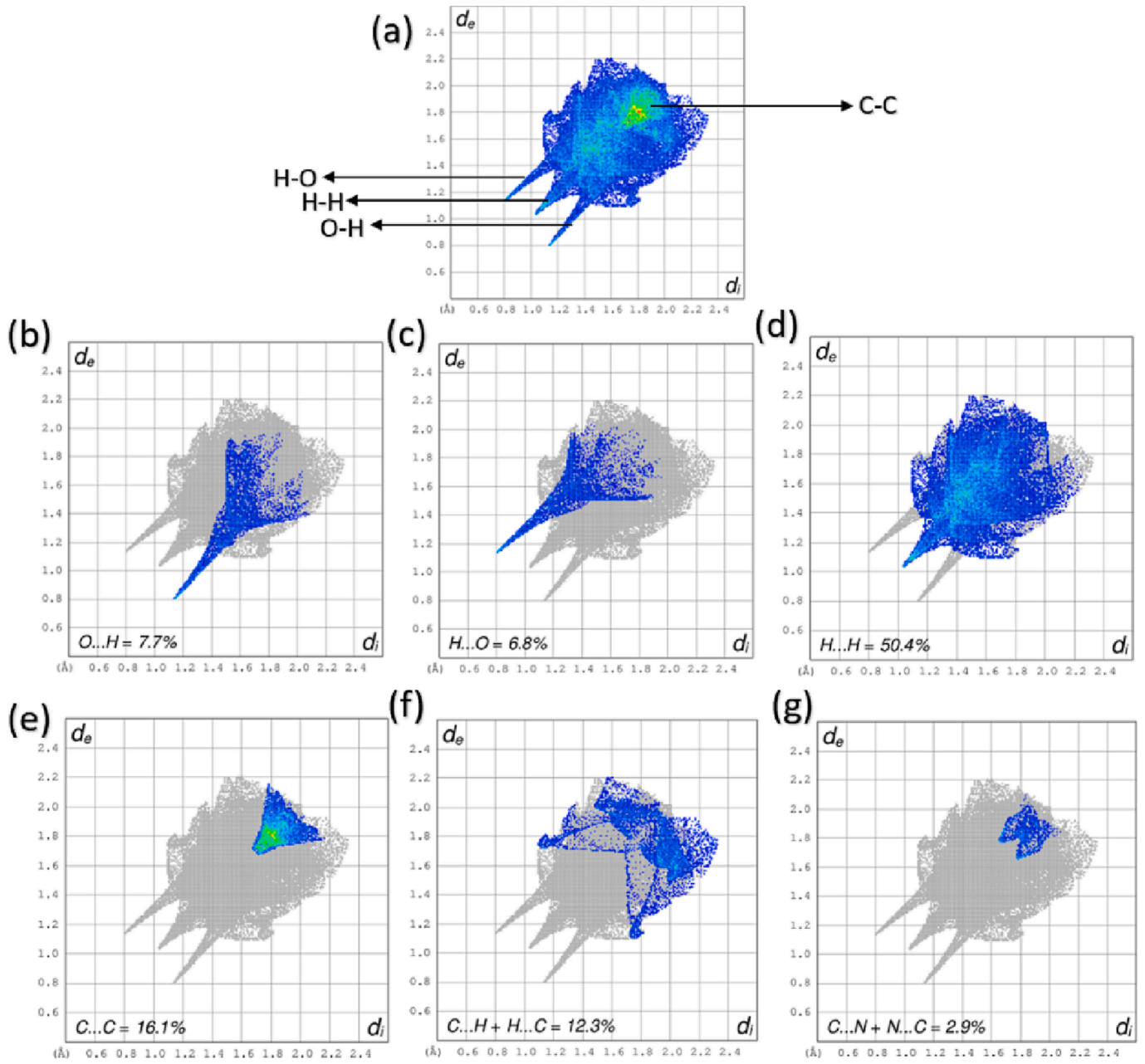

Fig. 8. 2D fingerprint plots of 2,9-DMQA indicating the contribution of intermolecular interactions of, (a) 2,9-DMQA molecule, (b) O…H, (c) H…O, (d) H…H, (e) C…C, (f) C…H + H…C, (g) C…N + N…C.

contribute in the excitation of the charges. That's the reason there is an unavailability of transition density for the hydrogen atoms. The TDM plot of the title compound is illustrated in Fig. 6 (A). The TDM plot indicates the high accumulation of charge density nearby the oxygen and nitrogen atoms symmetrically near the lower diagonal area. The lower left corner of the heat map has a large value area, which corresponds to the N – H and C = O bonds. This can be interpreted as the hole and electron must have large distribution nearby the N – H and C = O bonds. The sites (1,4) are highly positive which results in a positive contribution to the transition dipole moment of the X component. This reveals the availability of the charge density nearby these bonds and their active participation in charge transport. The outcomes from the TDM plot were supported by the isosurface map shown in Fig. 6 (B). This significant positive contribution of the N – H and C = O bonds in the density matrix plot can be considered as the reason for the green isosurfaces nearby atoms 1O, 2O, 3 N, and 4 N. Additionally, the higher order hydrogen atoms doesn't impart in isosurface formation. The binding energy was also computed for the title molecule. Therefore, the TDM analysis reports the potential candidature of C = O and N – H bonds as electron-withdrawing and donating moieties respectively.

3.5. Hirshfeld surface and 2D fingerprint plots analysis

Hirshfeld's surface (Fig. 6) was computed for 2,9-DMQA to visualize and study the intermolecular interactions of the molecular crystal. The red regions in Fig. 6 indicate the close contact between the nearest neighbouring atoms [49]. This can be interpreted as the area with higher hydrogen bond interactions. The red surface around the N – H and C = O bonds indicates the compactness in the bonds of bonds and higher intermolecular interactions that will be induced due to the presence of these bonds. 2D-fingerprint plots were also drawn for 2,9-DMQA to provide a visual summary of the frequency of each combination of *de*

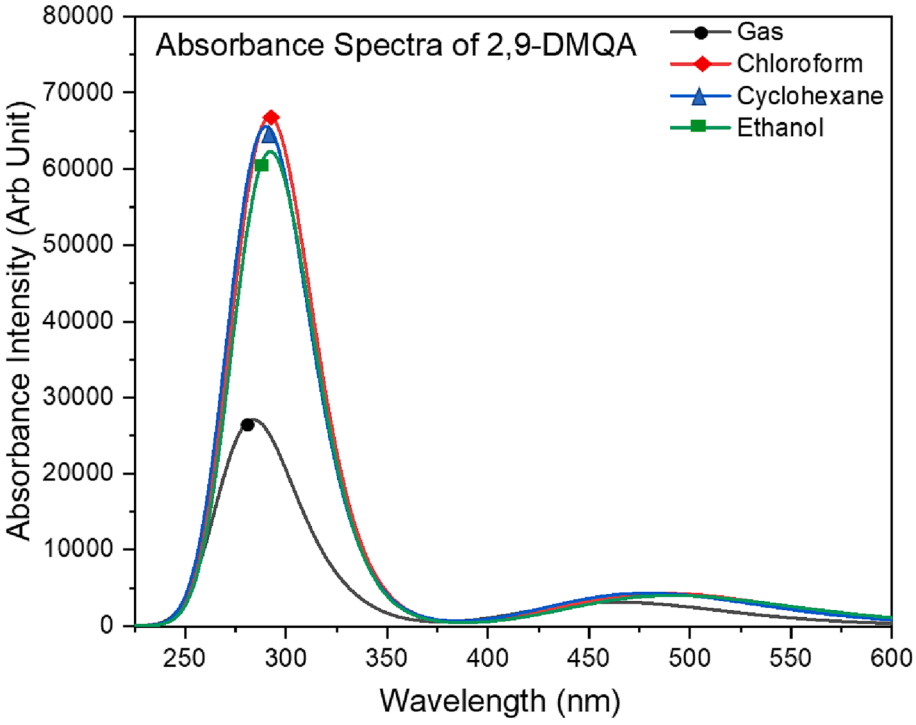

Fig. 9. Absorption spectra of 2,9-DMQA in the gas phase, chloroform, cyclohexane, and ethanol solvent.

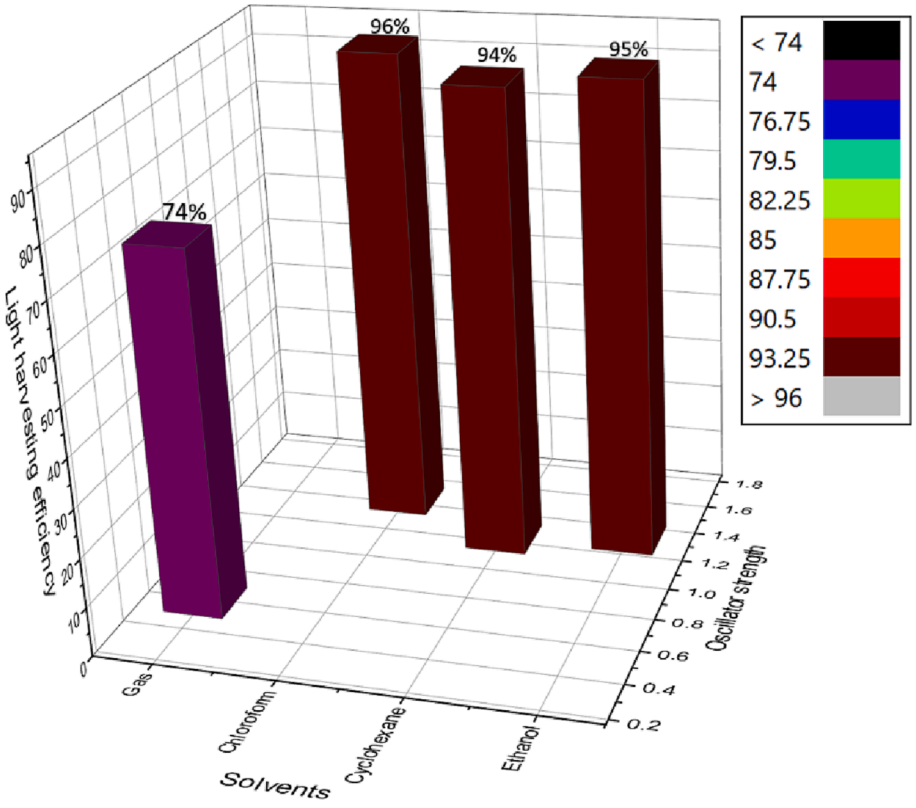

Fig. 10. Graph showing LHE of the 2,9-DMQA in different solvents.

and *di* across the surface of a molecule, so they not only indicate which intermolecular interactions are present but also the relative area of the surface corresponding to each kind of interactions [50]. Fig. 7(a) illustrates the 2D fingerprint plot of 2,9-DMQA and Fig. 7(b),….,(e) shows the individual contributions of the intermolecular interactions between atoms. The largest contribution to the overall crystal packing in the compound is from H···H interactions i.e., 50.4%. C…C interactions are the second largest contributory interactions in the intermolecular interactions and impart 16.1% to the total intermolecular interactions. The dominant H…H hydrogen bonding interactions exhibited a distinct

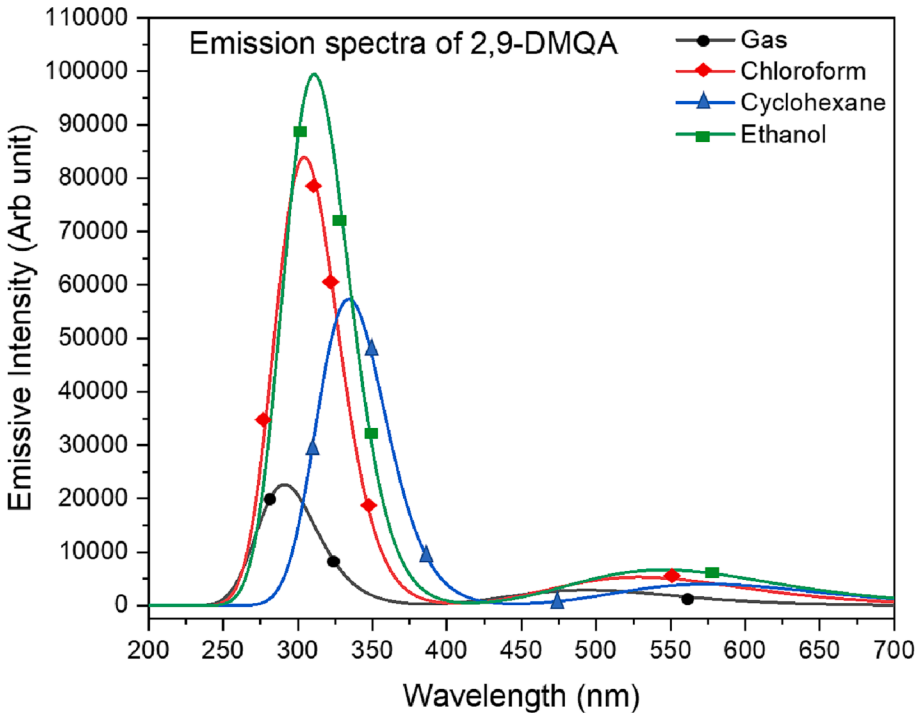

Fig. 11. Emission spectra for the 2,9-DMQA in the gas phase, chloroform, cyclohexane, and ethanol solvent.

spike in the middle of the 2D fingerprint plots, shown in Fig. 7. The uppermost major peak was due to the 6.8% contribution of H…O interactions and the lowest peak in the fingerprint plot was observed due to the 7.7% contribution of O…H interactions. C…H + H…C contributed 12.3% to the total fingerprint plot of 2,9-DMQA.

3.6. Absorption and light harvesting studies

The absorption spectrum of 2,9-DMQA in the gas, chloroform, cyclohexane, and ethanol solvent was computed using TD-DFT and the spectra were illustrated in Fig. 8 and all the transition details including wavelength, oscillator strength (*f*), and excitation energy (*E*) had been listed in SD 4. A broad absorption spectrum of 2,9-DMQA in the gas phase was observed between 250 and 530 nm with its crucial transition $S_0 \rightarrow S_9$ at 281 nm ($f = 0.5916$). After the introduction of the solvents (chloroform, cyclohexane, and ethanol), the absorption band shifted to the range of 280–550 nm. However, there was no significant difference in the absorption band of the 2,9-DMQA in all the considered solvents. The peak of the absorption spectra of 2,9-DMQA in chloroform, cyclohexane, and ethanol was observed at 291, 291, and 289 nm with *f* values 1.4319, 1.2331, and 1.3202 for crucial transition $S_0 \rightarrow S_7$ respectively. However, the transition wavelength was high (and equal) for chloroform and ethanol with no significantly distinguishing values of *E* and *f*. The absorption analysis indicates that there was a hyperchromatic shift in the absorption spectra after the introduction of the solvents. The results were comparatively promising for ethanol. Moreover, the shifting of the spectra was due to the shifting of the charge cloud from the HOMO-LUMO. The shifting of the absorption spectra indicates the participation of solvents in inducing intramolecular interactions [51]. The absorption spectra of 2,9-DMQA indicate the existence of typical $\pi \rightarrow \pi^*$ transitions. Thus, the existence of such transitions reported that 2,9-DMQA is chemically active to induce ICT.

The LHE of the title molecule computed using equation (12) was shown in Fig. 9. The *f* value of 0.5916 ($S_0 \rightarrow S_9$) gave the value of 0.74. this shows that 74% of incident light can be converted into electricity. The *f* values rise to 1.4319, 1.2331, and 1.3202 for chloroform, cyclohexane, and ethanol. This leads to a tremendous rise in LHE of the title molecule up to 96, 94, and 95% for chloroform, cyclohexane, and ethanol respectively. However, the LHE of the title molecule in solvents increases as $(LHE)_{gas} < (LHE)_{cyclohexane} < (LHE)_{ethanol} < (LHE)_{chloroform}$. Therefore, the LHE indicates the potential candidature of 2,9-DMQA as effective photosensitizing material in DSSCs for converting light energy to electrical energy [52].

3.7. Emission and radiative lifetime studies

Like absorption, a broad emission band (Fig. 10) between 250 and 375 nm was obtained for 2,9-DMQA in the gas phase. However, there was a bathochromic shift in the wavelength of the emission spectra of the 2,9-DMQA in all the considered solvents. The crucial transition $S_0 \rightarrow S_7$ of chloroform, cyclohexane, and ethanol was observed at wavelength 295, 301, and 290 nm respectively. The rise in the values of *f* was also observed for the considered solvents. The values of *f* for chloroform, cyclohexane and ethanol were computed as 2.0347, 1.2104, and 2.3061 respectively. However, the value of *f* was highest for ethanol indicating the highest ability of the emissive transitions of 2,9-DMQA in the ethanol phase. The emissive spectra of the title molecule were in the acceptable range indicating the fluorescent nature of 2,9-DMQA in considered solvents. The *f* values obtained for the crucial transitions were used for calculating the τ of the 2,9-DMQA in all the considered solvents (using equation (13). The values of τ less than 10 ns are referred to as radiative transitions and the transitions having values greater than 10 ns are categorized as non-radiative in nature [53]. τ for 2,9-DMQA in gas, chloroform, cyclohexane, and ethanol were computed as 1.18, 0.37, 0.35, and 0.6 respectively. All values are lower than 10 ns and are thus known to be radiative in nature. This shows that these transitions eject energy in the form of photons. Thus, the crucial emissive transitions of 2,9-DMQA are radiative in nature.

3.8. Adsorption with TiO_2 surface

TiO_2 is the most commonly used active material in solar cell applications that acts as an efficient energy harvesting layer in solar cells. TiO_2 has a ΔE of 3.2 eV which allows the effective absorption of UV light.

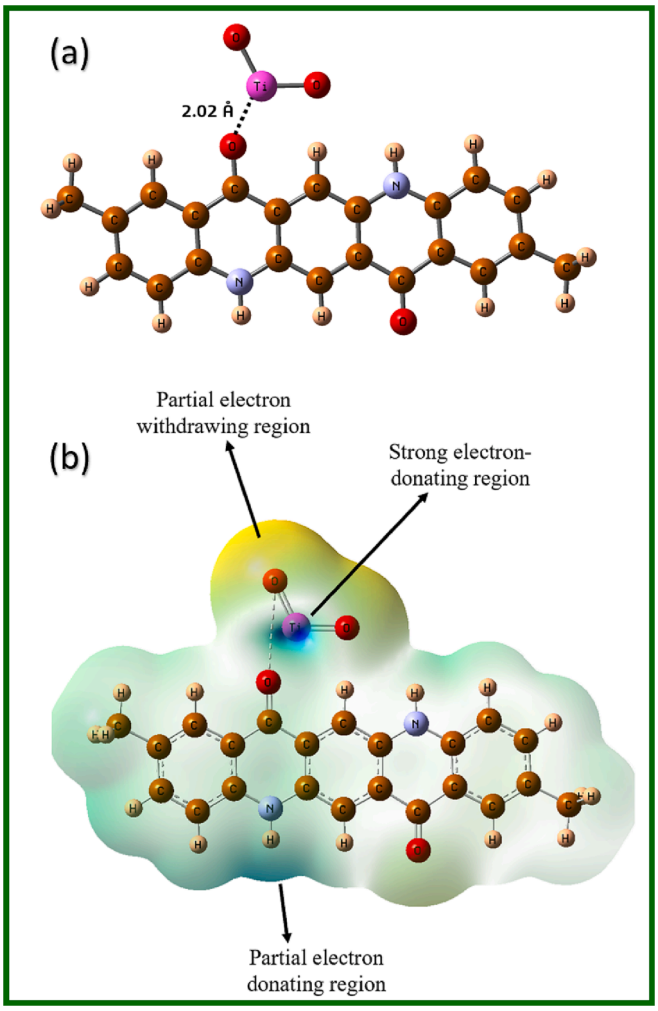

Fig. 12. (a) Optimized geometry of 2,9-DMQA and TiO_2 showing the interaction between both fragments, (b) MEP surface of 2,9-DMQA + TiO_2 indicating the involvement of TiO_2 in charge transfer.

Thus, the narrow ΔE provides a broad absorbance wavelength to the solar cell. Numerous studies in the literature have been reported on TiO_2 as a metal oxide semiconductor. M. Hachi and their team used DFT and TD-DFT calculations for the photovoltaic properties of the π-bridge indole derivative [41]. S. Mandal and the team have used TiO_2 surface as adsorbate for triphenylamine-based dyes for their computational study. the complex has been used as an efficient photosensitizer for photovoltaics [53]. Therefore, it is an ideal semiconductor for solar cells. Thus, the interactions between the title compound and TiO_2 have been studied to support the fabrication methods of the solar cell. The interaction energy between the 2,9-DMQA and TiO_2 was computed as 493440.86 kcal/mol. TiO_2 in the optimized geometry of the complex (2,9-DMQA + TiO_2) was located near the C = O bond of 2,9-DMQA. The bond length between Ti and O atoms was 2.02 Å. The higher the bond length, the more electrons holding the atoms together, and therefore the greater the stability. Moreover, the higher bond length leads to an increment in the polarity, and hence the dipole moment increases. Thus, a significant rise in the dipole moment of the complex (11.28 Debye) was observed due to the bond length between 2,9-DMQA and TiO_2. Therefore, the bond between the fragments and the dipole interactions reflects the occurrence of adsorption between 2,9-DMQA and TiO_2. The adsorption between the 2,9-DMQA and TiO_2 was computed to support the interaction between both fragments. 2,9-DMQA (dye) adsorption energy over the TiO_2 was obtained as 21397.62 eV (493.440.9 kcal/mol). The MEP surface illustrated in Fig. 11(b) was shown to indicate the nucleophilic and electrophilic region of the complex. The dark blue color over the Ti atom of TiO2 indicates the strong electron-donating tendency of TiO_2. The HOMO-LUMO surface seemed to support the MEP surface better. The orbital surfaces were seen to dislocate above 2,9-DMQA molecule in LUMO from TiO_2 in HOMO (Fig. 12). This validates the involvement of TiO_2 in charge transfer. Moreover, the computed ΔE was best for ethanol solvent (2.88 eV), but after the adsorption of TiO_2, a significant decrement in the ΔE of the complex was observed. The ΔE of the complex was computed as 2.22 eV. In order to become an ideal semiconductor for the considered dye (2,9-DMQA), the energy of the LUMO of 2,9-DMQA should be higher than the energy of HOMO of TiO_2. In the present study, the $LUMO_{2,9\text{-}DMQA}$ (-2.71 eV) > $HOMO_{TiO2}$ (-3.45 eV). Thus, the overall analysis of 2,9-DMQA with TiO_2 validates the potential behavior of TiO_2 as an ideal semiconductor to inject electrons.Fig. 13.

3.9. Photovoltaic and charge transport properties analysis

V_{OC} is one of the parameters that have a major influence on the photovoltaic activity of the material. The computed values of V_{OC} for the title molecule in different phases have been mentioned in Table 3. The value of V_{OC} can be calculated as energy difference between the energy of the lowest unoccupied molecular orbital (LUMO) of the 2,9-DMQA (dye) and the conduction band (E_{CB}) of the semiconductor TiO_2 (Table 3). In the gas phase, the value of V_{OC} was maximum and the values of V_{OC} for solvents are as V_{OC} (cyclohexane) > V_{OC} (chloroform) > V_{OC} (ethanol) (Table 3). The V_{OC} in cyclohexane was the highest. The obtained values of V_{OC} for 2,9-DMQA in different solvents vary from 0.74 eV (ethanol) to 1.11 eV (gas). These values are promising to reflect the possibility of electron injection among the donor and acceptor moiety. Moreover, the values of V_{OC} in our case are comparable to that reported by Zouhair *et al.* [54], A. Aboulouard *et al.* [39], Hachi *et al.* [41], and S. Mandal *et al.* [53]. The *FF* was also calculated to check the potential application of the material in photovoltaics. *FF* is the function of a dimensionless voltage expressed in equation (19). The calculated values of V_d are mentioned in Table 3. The value of *FF* in different solvents was observed as *FF* (gas) > *FF* (cyclohexane) > *FF* (chloroform) > *FF* (ethanol) (Table 3). The title compound 2,9-DMQA has the highest values of *FF* in cyclohexane solvent. Thus, the photovoltaic parameters have promising value in cyclohexane solvent. This might be due to the lowest angle and torsional strain of cyclohexane that give rise to the staggered conformation of the cyclohexane geometry. The staggered conformation of cyclohexane results in more stable bond formation between the dye and TiO_2. There is no such staggered conformation in chloroform and ethanol. Moreover, the volatile nature of chloroform and ethanol might be a reason for least contribution of the solvents in the bond formation between the dye and TiO_2. The observed values of *FF* in the present study are good enough to prove the photosensitizing activity in the considered material. Moreover, these values are comparable to the comparable to *FF* values computed in A. Aboulouard *et al.* [39]. Therefore, all the photovoltaic parameters reveal that 2,9-DMQA can be used as sensitizers because the electron injection process between 2,9-DMQA and TiO_2 and subsequent regeneration is possible in a dye-sensitized solar cell.

4. Conclusion

The DFT calculations performed in the present paper report the potential photovoltaic characteristics of 2,9-DMQA in the gas phase as well as in three different solvents i.e., chloroform, cyclohexane, and ethanol. The ΔE was found to be minimum for the gas phase followed by cyclohexane, chloroform, and ethanol solvents. The chemical hardness was also found to be highest for the gas phase. To identify the reactive sites of the molecule, MEP surface, *IP* surface, and counterplots were observed. These surfaces identified the C = O and N – H groups as the reactive sites within the 2,9-DMQA. This prediction was better supported by the NBO

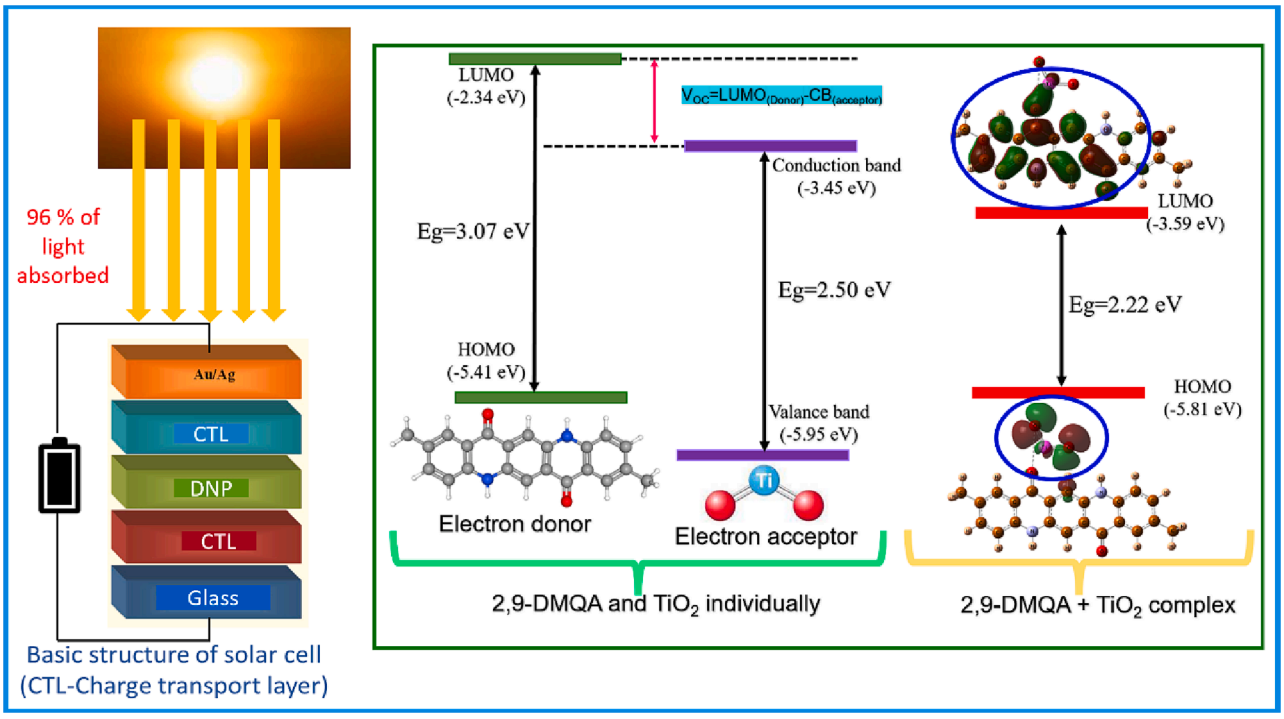

Fig. 13. Figure illustrating the photovoltaic application of 2,9-DMQA (present research study). Inset Scheme shows the concept of open circuit voltage calculation done in the present study. The ΔE of 2,9-DMQA and TiO_2 and the decrement in the ΔE and in the 2,9-DMQA + TiO_2 complex state are shown. HOMO-LUMO map of 2,9-DMQA + TiO_2 showing the dislocation of surfaces between TiO_2 and 2,9-DMQA.

Table 3
Computed photovoltaic parameters for the gas phase, and chloroform, cyclohexane, and ethanol solvent (V_{OC} in volt (V), V_d and *FF* are dimensionless).

Parameters Solvents	V_{OC}	V_d	*FF*
Gas	1.11	43.15	0.891
Chloroform	0.797	30.98	0.860
Cyclohexane	0.877	34.09	0.870
Ethanol	0.74	28.76	0.852

analysis when the interactions between the mentioned groups were observed with high stabilization energy. The fingerprint print plots were determined to identify the contribution of the intramolecular interactions. The absorption spectra better support the ICT between the C = O and N – H groups. Moreover, the computed value of light harvesting efficiency was also higher for the title compound showing its enhanced application as a potential absorber for solar cells. The emission spectra account for the radiative nature of the transitions. The ω of 2,9-DMQA reflects the donating nature of the compound. The interaction of the title molecule with TiO_2 was also promising. The value of the Eg was seen to decrease after the introduction of TiO_2. Moreover, the dislocation of HOMO-LUMO surfaces between TiO_2 and 2,9-DMQA enhances the interactions between the donor and acceptor moieties. The values for *Voc* was obtained between 0.74 V and 1.11 V for different solvents. The high value of the fill factor (less than0.8 for all solvents) was also promising enough to show the potential characteristics of 2,9-DMQA as an efficient solar cell material. Therefore, the present study claims the title molecule as an active material in solar cell applications, and the study can be a strong basis for the experimental demonstrations of the desired properties of the title molecule. The presented study might be fruitful in providing a new strategy and guidance for experimental scientists to synthesize new photosensitizing dye from the title compound. Furthermore, the excellent performance of the proposed dye can be used in various optoelectronic applications.

Ethical approval

I give my consent for the publication of identifiable details, which include data and pictures to be published in the Journal.

Funding

The authors declare that this research received no specific grant from any funding agency.

CRediT authorship contribution statement

Shradha Lakhera: Writing – original draft, Methodology, Data curation, Conceptualization, Visualization, Validation. **Meenakshi Rana:** Supervision, Methodology, Conceptualization, Software, Visualization, Writing – review & editing. **Kamal Devlal:** Supervision, Conceptualization, Formal analysis. **N. Kanagathara:** Software, Formal analysis. **Jan Janczak:** Visualization, Validation, Software, Formal analysis.

Declaration of Competing Interest

The authors declare that they have no known competing financial interests or personal relationships that could have appeared to influence the work reported in this paper.

Data availability

No data was used for the research described in the article.

Appendix A. Supplementary data

Supplementary data to this article can be found online at https://doi.org/10.1016/j.jphotochem.2023.114664.

References

[1] Y.S. Mary, T.E. Bolelli, R. Thomas, A.R. Krishnan, K. Bolelli, E.N. Kasap, T. Onkol, I. Yildiz, Quantum Mechanical Studies of Three Aromatic Halogen-Substituted Bioactive Sulfonamidobenzoxazole Compounds with Potential Light Harvesting Properties, Polycycl Aromat Compd. (2019) 10.1080/10406638.2019.1689405.

[2] P.C. Ray, Size and shape dependent second order nonlinear optical properties of Nanomaterials and their applications in biological and chemical sensing, Chem. Rev. 110 (9) (2010) 5332–5365, https://doi.org/10.1021/cr900335q.

[3] N. Wazzan, R.M. El-Shishtawy, A. Irfan, DFT and TD–DFT calculations of the electronic structures and photophysical properties of newly designed pyrene-core arylamine derivatives as hole-transporting materials for perovskite solar cells, Theor Chem Acc 137 (1) (2018).

[4] B. Nagarajan, S. Kushwaha, R. Elumalai, S. Mandal, K. Ramanujam, D. Raghavachari, Novel ethynyl-pyrene substituted phenothiazine based metal free organic dyes in DSSC with 12% conversion efficiency, J. Mater. Chem. A 5 (2017) 10289–10300, https://doi.org/10.1039/C7TA01744H.

[5] T. Shree, M. Chandra, Rajendra, Renewable Energy: World's Most Required Technique for Electricity, Turkish Online Journal of Qualitative Inquiry, 12 (9) (2021) e 9, p5664-5676. 13p. https://web.s.ebscohost.com/abstract?direct=true&profile=ehost&scope=site&authtype=crawler&jrnl=13096591&AN=160604901&h=vEwEPzWVXwg0aCKWls1ZWuoZaG8Xso9LuFZjbZHPn0JTnYE528KgH5QzlcjrijfEn4kpVlCAEJX%2bh2Yx40sNJw%3d%3d&crl=c&resultNs=AdminWebAuth&resultLocal=ErrCrlNotAuth&crlhashurl=login.aspx%3fdirect%3dtrue%26profile%3dehost%26scope%3dsite%26authtype%3dcrawler%26jrnl%3d13096591%26AN%3d160604901.

[6] J.L. Brédas, D. Beljonne, V. Coropceanu, J. Cornil, Charge-Transfer and Energy-Transfer Processes in π-Conjugated Oligomers and Polymers: A Molecular Picture, Chem. Rev. 104 (2004) 4971−5003. https://doi.org/10.1021/cr040084k.

[7] A. Pandey, S. Bhattacharya, J. Panigrahi, S. Mandal, V.K. Komarala, Effect of Gas Flow Rate in PECVD of Amorphous Silicon Thin Films for Interface Passivation of Silicon Heterojunction Solar Cells, Appl. Mater. Sci. 219 (16) (2022) 2200183.

[8] M.S. Abusaif, M. Fathy, M.A. Abu-Saied, A.A. Elhenawy, A.B. Kashyout, M. R. Selim, Y.A. Ammar, New carbazole-based organic dyes with different acceptors for dye-sensitized solar cells: Synthesis, characterization, dssc fabrications and density functional theory studies, Journal of Molecular Structure 1225 (2021) 129297.

[9] Q.-X. Tong, S.-L. Lai, M.-Y. Chan, K.-H. Lai, J.-X. Tang, H.-L. Kwong, C.-S. Lee, S.-T. Lee, High Tg Triphenylamine-Based Starburst Hole-Transporting Material for Organic Light-Emitting Devices, Chem. Mater. 19 (24) (2007) 5851–5855.

[10] J. Sarrato, A.L. Pinto, G. Malta, E.G. Röck, J. Pina, J.C. Lima, A.J. Parola, P. S. Branco, New 3-Ethynylaryl Coumarin-Based Dyes for DSSC Applications: Synthesis, Spectroscopic Properties, and Theoretical Calculations, Molecules. 26 (10) (2021) 2934, https://doi.org/10.3390/molecules26102934.

[11] N. Duvva, L. Giribabu, Hexyl dithiafulvalene (HDT)-substituted carbazole (CBZ) D–π–A based sensitizers for dye-sensitized solar cells, New J. Chem. (2020), https://doi.org/10.1039/D0NJ04147E.

[12] M. Malagoli, J.L. Brédas, Density functional theory study of the geometric structure and energetics of triphenylamine-based hole-transporting molecules, Chem. Phys. Lett. 327 (1–2) (2000) 13–17, https://doi.org/10.1016/S0009-2614(00)00757-0.

[13] A. Mahmood, J. Yang, J. Hu, X. Wang, A. Tang, Y. Geng, Q. Zeng, E. Zhou, Introducing Four 1,1-Dicyanomethylene-3-indanone End-Capped Groups as an Alternative Strategy for the Design of Small-Molecular Nonfullerene Acceptors, J. Phys. Chem. 122 (51) (2018) 29122–29128, https://doi.org/10.1021/acs.jpcc.8b09336.

[14] A. Mahmood, J. Hu, A. Tang, F. Chen, X. Wang, E. Zhou, A novel thiazole-based acceptor for fullerene-free organic solar cells, Dyes, and Pigments 149 (2018) 470–474, https://doi.org/10.1016/j.dyepig.2017.10.037.

[15] M. Haroon, M.R.S.A. Janjua, Exploring the effect of end-capped modifications of carbazole-based fullerene-free acceptor molecules for high-performance indoor organic solar cell applications, J. Comput. Electron. 21 (2022) 40–51, https://doi.org/10.1007/s10825-021-01838-w.

[16] M. Haroon, A. A. Al-Saadi, M. R. S. A. Janjua, Insights into end-capped modifications effect on the photovoltaic and optoelectronic properties of S-shaped fullerene-free acceptor molecules: A density functional theory computational study for organic solar cells, 35 (4) (2022) e4314. https://doi.org/10.1002/poc.4314.

[17] S. Lakhera, M. Rana, K. Devlal, Investigation of the Electrical and Optical Activity of Halogen-substituted 2-nitrotoulene by Density Functional Theory (2022). https://doi.org/10.21203/rs.3.rs-2111123/v1.

[18] S. Lakhera, M. Rana, K. Devlal, Theoretical study on spectral and optical properties of essential amino acids: a comparative study, Opt Quantum Electron. 54 (2022) 714, https://doi.org/10.1007/s11082-022-04118-4.

[19] S. Lakhera, M. Rana, K. Devlal, I. Celik, R. Yadav, A comprehensive exploration of pharmacological properties, bioactivities and inhibitory potentiality of luteolin from Tridax procumbens as anticancer drug by in-silico approach, Struct. Chem. (2022), https://doi.org/10.1007/s11224-022-01882-7.

[20] M.R.S.A. Janjua, Photovoltaic properties and enhancement in near-infrared light absorption capabilities of acceptor materials for organic solar cell applications: A quantum chemical perspective via DFT, Journal of Physics and Chemistry of Solids. 171 (2022), 110996, https://doi.org/10.1016/j.jpcs.2022.110996.

[21] M.U. Khan, R. Hussain, M. Yasir Mehboob, M. Khalid, Z. Shafiq, M. Aslam, A.A. Al-Saadi, S. Jamil, M.R.S.A. Janjua, In Silico Modeling of New "Y-Series"-Based Near-Infrared Sensitive Non-Fullerene Acceptors for Efficient Organic Solar Cells, ACS Omega 5 (37) (2020) 24125–24137.

[22] M.R.S.A. Janjua, Prediction and Understanding: Quantum Chemical Framework of Transition Metals Enclosed in a $B_{12}N_{12}$ Inorganic Nanocluster for Adsorption and Removal of DDT from the Environment, Inorg. Chem. 60 (14) (2021) 10837–10847, https://doi.org/10.1021/acs.inorgchem.1c01760.

[23] M.R.S.A. Janjua, How Does Bridging Core Modification Alter the Photovoltaic Characteristics of Triphenylamine-Based Hole Transport Materials? Theoretical Understanding and Prediction. 27 (12) (2021) 4197–4210, https://doi.org/10.1002/chem.202004299.

[24] C. Wang, Z. Zhang, Y. Wang, Quinacridone-based π-conjugated electronic materials, J. Mater. Chem. C 4 (2016) 9918–9936, https://doi.org/10.1039/C6TC03621J.

[25] Y. Saito, S. Iwamoto, Y. Tanaka, N. Hontama, T. Endo, Suppressing aggregation of quinacridone pigment and improving its color strength by using chitosan nanofibers, Carbohydrate Polymers. 255 (2021), 117365, https://doi.org/10.1016/j.carbpol.2020.117365.

[26] H. Meier, W. Albrecht, Photoelectric Properties of 2,9-Dimethyl-quinacridone, Zeitschrift fur Physikalische Chemie Neue Folge 148 (1986) 171–183.

[27] K. Manabe, S. Kusabayashi, M. Yokoyama, Long-life Organic Solar Cell Fabrication Using Quinacridone Pigment, Chem. Lett. 16 (4) (1987) 609–612.

[28] N.M. O'Boyle, M. Banck, C.A. James, C. Morley, T. Vandermeersch, G. R. Hutchison, Open Babel: An open chemical toolbox, J Cheminform 3 (1) (2011), https://doi.org/10.1186/1758-2946-3-33.

[29] M. J. Frisch: Gaussian 09, Revision B.01, Gaussian Inc., Wallingford CT. (2010).

[30] A.D. Becke, Density-functional thermochemistry. V. Systematic optimization of exchange-correlation functionals, J. Chem. Phys. 107 (1997) 8554–8560, https://doi.org/10.1063/1.475007.

[31] Y. Shao, L.F. Molnar, Y. Jung, J. Kussmann, C. Ochsenfeld, S.T. Brown, Phys. Chem. Chem. Phys. 8 (2006) 3172.

[32] T. Koopmans, Ordering of wave functions and eigenenergies to the individual electrons of an atom, Physica. 1 (1933) 104–113, https://doi.org/10.1016/S0031-8914(34)90011-2.

[33] N.M. O'Boyle, A.L. Tenderholt, K.M. Langner, J. Comp. Chem. 29 (2008) 839–845.

[34] T. Lu, F. Chen, Multiwfn: A Multifunctional Wavefunction Analyzer, J. Comput. Chem. 33 (2012) 580–592, https://doi.org/10.1002/jcc.22885.

[35] A. Özarslan, D. Çakmaz, F. Erol, H. Şenöz, N. Seferoğlu, A. Barsella, Z. Seferoğlu, Synthesis and investigation of photophysical, NLO and thermal properties of D-π-A-π-D dyes, J. Mol. Struct. 1229 (2021) 129583.

[36] S. Lakhera, K. Devlal, M. Rana, V. Dhuliya, Computational study of non-linear optical and electrical properties of 1,3-dinitropyrene, Opt. Quant. Electron. 55 (2023) 85, https://doi.org/10.1007/s11082-022-04371-7.

[37] M. Faizan, M. Mehkoom, Z. Afroz, V.H.N. Rodrigues, S.M. Afzal, S. Ahmad, Experimental and computational investigation of novel dihydrated organic single crystal of 2,4,6-triaminopyrimidine and 3,5-dintrobenzoic acid: Linear and nonlinear optical response with limiting performance, J. Solid State Chem. 300 (2021), 122255, https://doi.org/10.1016/j.jssc.2021.122255.

[38] L. Zhang, X. Liu, W. Rao, J. Li, Multilayer Dye Aggregation at Dye/ TiO2 Interface via π…π Stacking and Hydrogen Bond and Its Impact on Solar Cell Performance: A DFT Analysis, Sci. Rep. 6 (2016) 35893, https://doi.org/10.1038/srep35893.

[39] A. Aboulouard, S. Mtougui, N. Demir, A. Moubarik, M. E. idrissi, M. Can, New non-fullerene electron acceptors-based on quinoxaline derivatives for organic photovoltaic cells: DFT computational study, Synthetic Metals 279 (2021) 116846. https://doi.org/10.1016/j.synthmet.2021.116846.

[40] Y. Fu, T. Lu, Y. Xu, M. Li, Z. Wei, H. Liu, W. Lu, Theoretical screening and design of SM315-based porphyrin dyes for highly efficient dye-sensitized solar cells with near-IR light harvesting, Dyes and Pigments 155 (2018) 292–299.

[41] M. Hachi, S.E. Khattabi, A. Fitri, A.T. Benjelloun, M. Benzakour, M. Mcharfi, M. Hamidi, M. Bouachrine, FT and TD-DFT studies of the pi-bridge influence on the photovoltaic properties of dyes based on thieno[2,3-b]indole, J. Mater. Environ. Sci. 9 (4) (2018) 1200–1211, https://doi.org/10.26872/jmes.2017.9.4.132.

[42] S. Lakhera, K. Devlal, A. Ghosh, M. Rana, In silico investigation of phytoconstituents of medicinal herb 'Piper Longum' against SARS-CoV-2 by molecular docking and molecular dynamics analysis, Results in Chemistry. 3 (2021), 100199, https://doi.org/10.1016/j.rechem.2021.100199.

[43] S. Lakhera, K. Devlal, A. Ghosh, P. Chowdhury, M. Rana, Modelling the DFT structural and reactivity study of feverfew and evaluation of its potential antiviral activity against COVID-19 using molecular docking and MD simulations, Chem. Pap. 76 (5) (2022) 2759–2776.

[44] S. Lakhera, K. Devlal, M. Rana, I. Celik, Study of nonlinear optical responses of phytochemicals of Clitoria ternatea by quantum mechanical approach and investigation of their anti-Alzheimer activity with in silico approach, Struct Chem (2022), https://doi.org/10.1007/s11224-022-01981-5.

[45] M. Rana, N. Singla, A. Chatterjee, A. Shukla, P. Chowdhury, Investigation of nonlinear optical (NLO) properties by charge transfer contributions of amine functionalized tetraphenylethylene, Opt. Mater. 62 (2016) 80–89, https://doi.org/10.1016/j.optmat.2016.09.043.

[46] D.D.Y. Setsoafia, K.S. Ram, H.M. Rad, D. Ompong, V. Murthy, J. Singh, DFT and TD-DFT Calculations of Orbital Energies and Photovoltaic Properties of Small Molecule Donor and Acceptor Materials Used in Organic Solar Cells, J. Renewable Mater. 10 (10) (2022), https://doi.org/10.32604/jrm.2022.020967.

[47] N. Kanagathara, F. MaryAnjalin, V. Ragavendran, D. Dhanasekaran, R. Usha, R.G. S. Rao, M.K. Marchewka, Experimental and Theoretical (DFT) investigation of Crystallographic, Spectroscopic and Hirshfeld surface analysis of anilinium arsenate, J. Mol. Struct. 1223 (2021) 128965.

[48] Multiwfn − A Multifunctional Wavefunction Analyzer − Software Manual with tutorials and abundant examples in Chapter 4 Version 3.8 (dev). (2022). http://sobereva.com/multiwfn.

[49] W. Guerrab, H. Lgaz, S. Kansiz, J.T. Mague, N. Dege, M. Ansar, R. Marzouki, J. Taoufik, I.H. Ali, M. Chung Ill, Y. Ramli, Synthesis of a novel phenytoin

derivative: Crystal structure, Hirshfeld surface analysis and DFT calculations, J. Mol. Struct. (2020), https://doi.org/10.1016/j.molstruc.2019.127630.
[50] M. Rana, P. Chowdhury, Effects of hydrogen bonding between pyrrole-2-carboxaldehyde and nearest polar and nonpolar environment, Spectrochim. Acta - A: Mol. Biomol. 185 (2017) 198–206, https://doi.org/10.1016/j.saa.2017.05.050.
[51] S. Lakhera, K. Devlal, M. Rana, V. Dhuliya, Quantum Mechanical Study of Three Aromatic Bioactive Fatty Alcohol Compounds with Nonlinear Optical and Potential Light Harvesting Properties, Opt. Mater. 129 (2022), 112476, https://doi.org/10.1016/j.optmat.2022.112476.
[52] S. Lakhera, M. Rana, K. Devlal, Influence of Adsorption of Gold and Silver Nanoclusters on Structural, Electronic, and Nonlinear optical properties of Pentacene-5, 12-dione: A DFT study, Opt. Quant. Electron. 55 (2023) 178, https://doi.org/10.1007/s11082-022-04422-z.
[53] S. Mandal, G.R. Kandregula, V.N.B. Tokala, A computational investigation of the influence of acceptor moieties on photovoltaic performances and adsorption onto the TiO2 surface in triphenylamine-based dyes for DSSC application, J. Photochem. Photobiol., A Chem. 401 (2020) 112745.
[54] Z. El Jouad, L. Cattin, M. Addou, J.C. Bernède, J.-M. Nunzi, R. Bennacer, M. El Ganaoui, M. El Jouad, Bernède Open circuit voltage of organic photovoltaic cells using C60 as acceptor: variation with the donor, Eur. Phys. J. Appl. Phys. 86 (2) (2019) 20201.